INORGANIC CHEMISTRY
FRONTIERS

RESEARCH ARTICLE

View Article Online
View Journal | View Issue

Cite this: *Inorg. Chem. Front.*, 2023, **10**, 692

Giant thermal expansion associated with a macroscopic polarization change in a single crystal of a Zn(II) complex†

Zheng Tang, [a] Chengdong Liu,[a] Yan Zhang,[a] Xiao-Peng Sun, [b] Jun Tao *[a] and Zi-Shuo Yao *[a]

In this study, we prepared a polar flexible single crystal of [Zn(4-ethylpyridine)$_2$(NCS)$_2$]. This material shows unusually large anisotropic linear thermal expansion as the tetrahedral coordination geometry of the complex can be modified in response to the thermal dynamic state of the ethyl group in 4-ethylpyridine ligands. Correspondingly, a giant thermally controlled reversible shape change of 10% elongation/contraction is observed in the rod-like single crystal along its long axis. Such a large thermal mechanical deformation is among the largest values in the reported thermal dynamic single crystals. Because the magnitude of dipole moment of uniaxially aligned molecules is varied by the large molecular structural change, the polarization of the single crystal is switched and manifests as a continuous pyroelectric current, particularly in the vicinity of phase transition points where molecular geometries are largely tuned. This study demonstrates that the large thermal expansion of flexible single crystals can be used to control the polarization of materials, providing a promising strategy to prepare superior pyroelectric materials.

Received 9th November 2022,
Accepted 27th November 2022

DOI: 10.1039/d2qi02371g

rsc.li/frontiers-inorganic

Introduction

Pyroelectric materials, whose internal polarization can be switched in response to a variation in temperature,[1–4] have been increasingly pursued for their fascinating applications in energy harvesting, heat sensing, and thermal imaging.[2,5–9] In the past few decades, numerous pyroelectric materials including triglycine sulfate (TGS), lithium tantalite ($LiTaO_3$), strontium barium niobate (SBN), lead zirconate titanate (PZT), polyvinylidene difluoride (PVDF), and their composites have been developed.[5] Among the different pyroelectric materials, molecule-based single crystals have attracted increasing attention for their environmental benignness, mild fabrication temperature, mechanical flexibility, and unambiguous structures characterized by single-crystal X-ray diffraction.[10–15] To date, research on molecule-based pyroelectric materials mainly focuses on molecular ferroelectrics.[10,11,15] Such materials typically generate substantial pyroelectric current in the vicinity of phase transition temperature but minute at other temperatures. Moreover, large polarization switching in ferroelectric materials usually needs to be preliminarily polarized by an external bias electric field because of crystal twinning, which is inappropriate for the practical application of pyroelectric properties.[11,16,17]

The structural origin of polarization switching is derived from the collective ionic displacement, molecular reorientation, and directional electron transfer.[10,11,18–22] In comparison to inorganic oxide materials, molecule-based materials possess intrinsic structural flexibility because their structures are built from molecular species connected *via* intermolecular interactions.[23–26] Recently, dozens of flexible single crystals with giant thermal expansion, thermal-induced electron transfer, or mechanical deformation have been developed.[23,26–31] If the thermally induced significant structural transformation is involved in the macroscopic polarization change of single crystals, a large pyroelectric response could be expected.

To this end, we focus our efforts on a flexible molecular crystal, [Zn(4-ethylpyridine)$_2$(NCS)$_2$] (**1**), that crystallized in a polar space group *Fdd*2. In our previous report, we have found that this single crystal shows outstanding plastic bending in

[a]*Key Laboratory of Cluster Science of Ministry of Education, School of Chemistry and Chemical Engineering, Liangxiang Campus, Beijing Institute of Technology, Beijing 102488, People's Republic of China. E-mail: taojun@bit.edu.cn, zishuoyao@bit.edu.cn*

[b]*Henan Key Laboratory of Polyoxometalate Chemistry, College of Chemistry and Chemical Engineering, Henan University, Kaifeng 475004, People's Republic of China*

†Electronic supplementary information (ESI) available: Experimental section, theoretical calculations, additional measurements, additional figures and tables (PDF). Crystal data for **1–3** at various temperatures (CIFs). Videos S1 and S2 for the reversible shape change of single crystal **1** (mp4). CCDC 2214726–2214732 and 2216171–2216174. For ESI and crystallographic data in CIF or other electronic format see DOI: https://doi.org/10.1039/d2qi02371g

response to external stress.[32] In the crystal, uniaxially aligned tetrahedral complexes underwent a substantial shape change (scissor-like motion) in their molecular structures in response to the thermal dynamic state change of ethyl groups. As the reorientation of 4-ethylpyridine ligands changed the molecular dimension, a large anisotropic linear thermal expansion that manifests as a reversible 10% expansion/contraction of rod-like single crystal was realized. Moreover, the molecular scissor-like motion changed the macroscopic polarization of single crystals, generating a continuous pyroelectric current along the polar axis of single crystals.

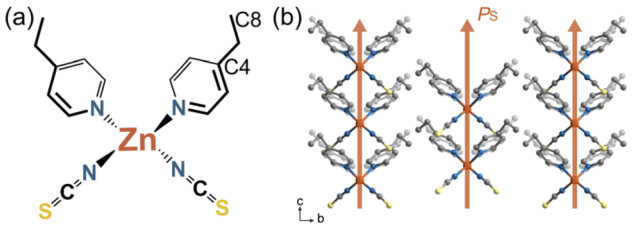

Fig. 1 Molecular structures of compound **1**. (a) Schematic of **1**. (b) Molecular packing viewed along the *a*-axis at 293 K. The brown arrows indicate the direction of spontaneous polarization. Colour code: Zn (brown), N (blue), C (grey), and S (yellow). Hydrogen atoms are omitted for clarity.

Experimental

Synthesis of [Zn(4-ethylpyridine)$_2$(NCS)$_2$] (1)

According to our previously reported method,[32] the rod-like single crystals of compound **1** were prepared by slow evaporation of an ethanol solution containing $Zn(ClO_4)_2{\cdot}6H_2O$, NH_4NCS and 4-ethylpyridine. Elemental analyses (%) calcd for **1**: 48.54, H, 4.58, N, 14.15. Found: C, 48.42, H, 4.61, N, 14.07.

Single-crystal X-ray diffraction

Variable-temperature single-crystal X-ray data of compound **1** at 90, 107, 150, 210, 260, 293, and 340 K were acquired using a Rigaku Oxford XtaLAB PRO diffractometer with Mo Kα (λ = 0.71073 Å) radiation. An Oxford Cryosystems Cryostream 800 apparatus was equipped to control the temperature with a nitrogen gas stream. The disordered structures at different temperatures were solved by a direct method and refined by full-matrix least-squares on F^2 using the SHELX program implemented in the Olex2 program with anisotropic thermal parameters for all non-hydrogen atoms.[33,34] All hydrogen atoms were added geometrically at calculated positions and refined by the riding model. Variable temperature crystallographic parameters for compound **1** are summarized in Table S1.† The full crystallographic data at different temperatures discussed in this study have been deposited at the Cambridge Crystallographic Data Centre (CCDC), under deposition numbers CCDC 2214726–2214732 and 2216171–2216174.†

Results and discussion

Crystal structure

In the crystal, Zn(II) ions are tetrahedrally coordinated by two N atoms from NCS^- anions and two N atoms from 4-ethylpyridine ligands (Fig. 1a). The metal centers lie in the crystallographic C_2 axis and the asymmetric unit contains half a Zn(II) ion, one 4-ethylpyridine, and one NCS^-. At room temperature, the 4-ethylpyridine ligands are heavily disordered over two positions as identified by the large thermal displacement parameters (Fig. S1†). The neutral complexes are further connected *via* weak π–π intermolecular interactions along the *c*-axis and C–H···S interactions (Fig. S2†), forming a three-dimensional (3D) structure. As all the polar molecules are uniaxially aligned along the crystallographic *c*-axis, compound **1** crystallizes in an orthorhombic polar space group *Fdd*2. Accordingly, spontaneous polarization emerges along the crystallography *c*-axis (Fig. 1b).

Thermal expansion

In this compound, the ligands of 4-ethylpyridine are coordinated in a disordered state, potentially actuating structural transitions under the stimulation of temperature as a result of disorder–order structural changes.[18,23,24,35] To determine the molecular motion and its effects on the cell parameters, we monitored the structural change in detail by variable-temperature single-crystal diffraction analysis. The data were collected in heating mode between 90 and 340 K (Table S1†), below the melting point of 370 K (Fig. S3†). A comparison of the molecular structures at different temperatures reveals that the thiocyanate anions are ordered in the measured temperature range, but the 4-ethylpyridine ligands are always disordered. As shown in Fig. 2, the ethyl group adopts two orientations. The different orientations of terminal groups modify the intermolecular interactions and then affect the coordination geometry of the complex. As a result, the aromatic plane of pyridine ligands is disordered over two positions. The temperature-dependent isotropic temperature factors of C8 (carbon atoms on the ethyl group) gradually increased from 90 to 340 K, indicating that the disorder of ethyl groups was enhanced by heating the sample (Fig. S4†). The variation in the thermal dynamic state not only tunes the orientation of the aromatic plane of pyridine ligands, but also changes the site occupancy factors (SOFs) of part A and B. As shown in Fig. 2 and S5,† the angle of C4(pyridine)–Zn–C4(pyridine) (*para*-carbon atoms of pyridine ligands) shifted from 106°/129° at 90 K to 106°/110° at 340 K, and the SOF of each disordered position, part A and B, significantly changed from 0.73/0.27 at 90 K to 0.43/0.57 at 340 K, respectively. Consequently, the average angle of C4–Zn–C4 presents a reversible change between 112° (90 K) and 108° (340 K). The dynamic motion of 4-ethylpyridine modifies the coordination sphere of the metal center. The angles of N(pyridine)–Zn–N(pyridine) and N(NCS)–Zn–N(NCS) shrank form 118° and 123° at 90 K to 112° and 120° at 340 K upon heating, respectively, but the lengths of the Zn–N coordination bond are almost

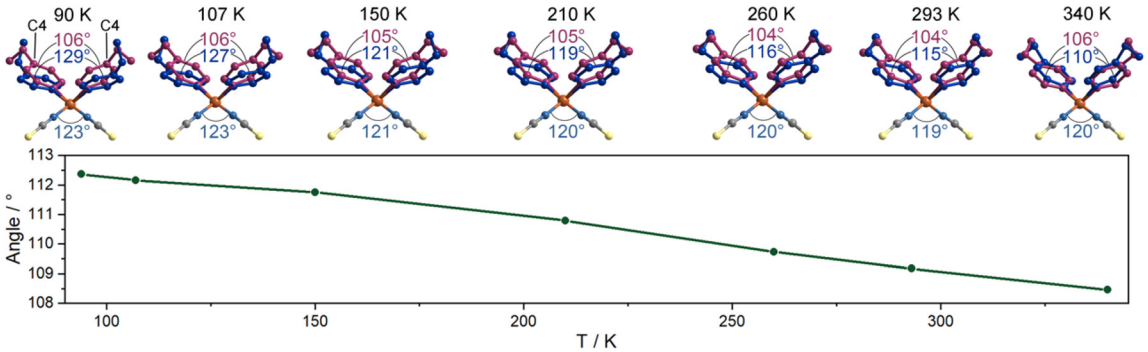

Fig. 2 Variation in the molecular structures and angles of C4–Zn–C4 (*para*-carbon atoms of pyridine ligands) in compound **1** in the temperature range of 90–340 K. The pink and deep blue atoms represent the structures of parts A and B in the disordered structure, respectively.

unchanged (2.026/1.930 Å at 90 K, 2.093/1.911 Å at 340 K, Fig. S1†). The substantial shifts in the coordination angles indicate the occurrence of a scissor-like motion at the molecular level of complex **1** (Fig. 2). Due to the uniaxially packed molecular structures and intermolecular interactions between the complexes, the molecular-level structural change is transduced into the unit cell of single crystals. As the temperature increased from 90 K to 340 K, the shortest Zn···Zn distance along the crystallographic *c*-axis increased from 4.8733(2) Å to 5.3374(5) Å, consistent with the closing motion of molecules upon heating (Fig. 3a). The scissor-like structural transformation of molecules was further supported by the contraction of the shortest Zn···Zn distance along the crystallographic *a*- and *b*-axes, *i.e.*, from 19.4675(8) and 39.9414(14) Å to 19.1290(2) and 39.5670(5) Å, respectively, as the temperature increased from 90 K to 340 K (Fig. S6†).

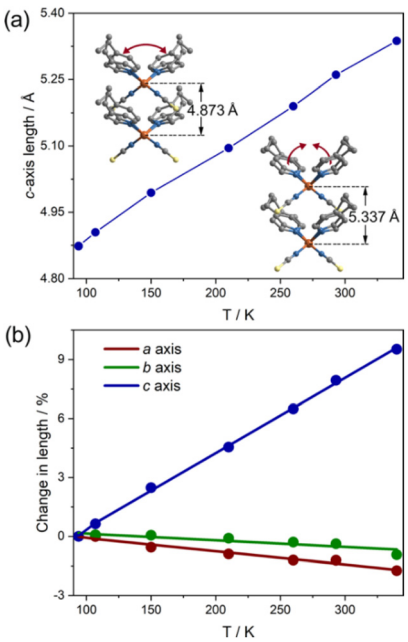

Fig. 3 Thermal expansion behaviour of compound **1**. (a) Temperature dependence *c*-axis length. (b) Linear thermal expansion coefficients calculated from *PASCal*.

The isotropic temperature factor of C8 and the angle of C4–Zn–C4 are almost linearly changed as the temperature varied. However, an anomaly was detected below 150 K. Differential scanning calorimetry (DSC) measurement was performed to investigate the possible phase transition of **1** in the low temperature range. As shown in Fig. S7 and S8,† two exothermic peaks at 112 and 99 K on the cooling process were detected in the DSC curve, and the corresponding endothermic peaks at 113 and 104 K on the heating process confirmed the reversible feature of the phase transitions. According to the single-crystal structural analyses, the polar space group *Fdd*2 was maintained during phase transition. Therefore, the phase transition should be ascribed to the structural deformation induced by the thermal dynamic state of ethyl groups. As shown in Fig. S5,† an abrupt change was detected in the SOF of parts A and B in the vicinity of phase transition point. The change in the C4–Zn–C4 angle during 90–150 K was also faster than that of variation during 150–340 K.

The change in the Zn···Zn distance manifests as a substantial variation in the cell parameters, upon heating from 90 to 340 K, the crystallographic *c*-axis expanded from 4.8733(2) to 5.3374(5) Å, whereas the *a*- and *b*-axes contracted from 19.4675(8) to 19.1290(2) Å and 39.9414(14) to 39.5670(5) Å, respectively (Fig. 3a, S9 and Table S1†), indicating *ca.* 9.5% expansion along the *c*-axis, −1.7% shrinkage along the *a*-axis, and −0.9% contraction along the *b*-axis. These changes exactly reflect the variations in the coordination geometry upon heating. Corresponding to the large expansion in the *c*-axial length, the unit-cell volume of the single crystal enlarged by 6.6% as the temperature increased from 90 to 340 K. The large volume implies that disordered 4-ethylpyridine may take various thermal dynamic states at the high temperature, particularly in the direction of *c*-axis. The linear variations on the crystallographic axes suggest a positive thermal expansion for *c*-axis and negative thermal expansion for *a*- and *b*-axes. As calculated from the program *PASCal*,[36] the linear thermal expansion coefficients along the principal axes of single crystals are 383 × 10^{-6} K^{-1} (α_c), −67 × 10^{-6} K^{-1} (α_a), and −34 × 10^{-6} K^{-1} (α_b),

respectively, in the temperature range of 90 to 340 K (Fig. 3 and S10†). Notably, no significant anomaly was detected in the thermal expansion coefficients near the phase transition points, implying that the abrupt variations in the SOF slightly affect the global structure of **1**. The thermal expansion coefficient of *c*-axis is much higher than those of typical ferroelectrics such as LiB_3O_5 (66.4×10^{-6} K^{-1})[37] and $Pb(Mg_{1/3}Nb_{2/3})O_3$–$0.3PbTiO_3$ (3.4×10^{-6} K^{-1}),[38] and similar to the values of some reported giant thermal expansion materials such as organic–inorganic hybrid complex ($(Himd)_2[CuCl_4]$, $\alpha_a = -38 \times 10^{-6}$ K^{-1}, $\alpha_b = 568 \times 10^{-6}$ K^{-1}, $\alpha_c = -184 \times 10^{-6}$ K^{-1}),[26] MOFs (FJI-H11-Et, $\alpha_a = -33.2 \times 10^{-6}$ K^{-1}, $\alpha_c = 489.4 \times 10^{-6}$ K^{-1}),[39] HOFs ($(H_4BPTC)\cdot(BPE)_2$, $125 \times 10^{-6} < \alpha_a < 394 \times 10^{-6}$, $-171 \times 10^{-6} < \alpha_b < -469 \times 10^{-6}$),[40] and organic crystalline material ((*S*, *S*)-octa-3,5-diyn-2,7-diol, $156 \times 10^{-6} < \alpha_a < 515 \times 10^{-6}$, $-32 \times 10^{-6} < \alpha_b < -85 \times 10^{-6}$, $-48 \times 10^{-6} < \alpha_c < -204 \times 10^{-6}$).[41]

Macroscopic mechanical response

The large anisotropic thermal expansion may induce a significant variation in the single crystal shape.[23,24,28,35,42–46] Hence, we monitored the deformation of a single crystal in response to the temperature change. The macroscopic shape change of a single crystal of **1** was examined using a microscope equipped with a heating–cooling temperature controller. On the basis of the face index of the single crystal, the long axis of the single crystal is parallel to the crystallographic *c*-axis (Fig. S11†). As shown in Fig. 4 and the ESI Videos S1 and S2,† the rod-like single crystal of **1** extended from 0.70 mm at 90 K to 0.77 mm at 340 K along the crystal long axis, and the thermally induced shape change can be recovered to its original shape upon cooling to 90 K. Notably, the reversible elongation/contraction of the single crystal can be repeated 10 cycles without any fracture detected in the single crystal surface, implying a good fatigue resistance of the large shape change. The good reproducibility of this single crystal should associate with the saddle stacking of the complexes along the *c*-axis, which can maintain the crystal lattice during the scissor-like motion, while the tension in the perpendicular directions was alleviated by the weak intermolecular interactions around the 1D molecular column. The *ca.* 10% elongation/contraction of single crystals is consistent with the variation in the crystallographic *c*-axial length in response to the temperature variation. The remarkably large shape of **1** is comparable to the large deformations of single crystals such as $[Ni^{II}(en)_3]ox$ (5%),[24] $(Himd)_2[CuCl_4]$ (10%),[26] 6,13-bis(triisopropylsilylethynyl)pentacene (10%),[35] and 2,7-di([1,1′-biphenyl]-4-yl)-fluorenone (18%) reported in the literature.[43] The materials with large temperature-dependent shape change are particularly useful for the development of precise thermomechanical actuators and sensors.[41,47,48]

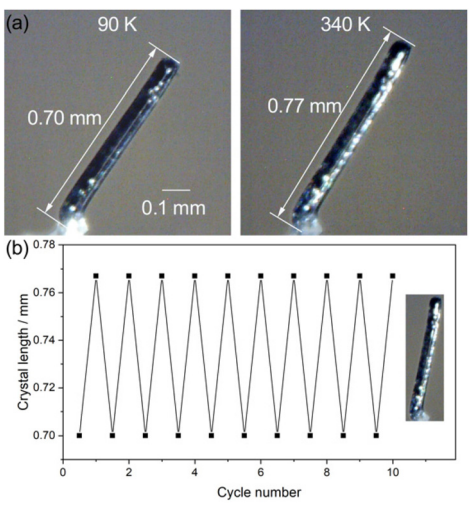

Fig. 4 Photographs of the crystal deformation of **1**. (a) Expansion and shrinkage of the rod-like single crystal in the temperature range of 90–340 K. According to the result of face index, the long axis of the single crystal is parallel to the crystallographic *c*-axis. The crystal length increased from 0.70 to 0.77 mm upon heating. (b) Fatigue resistance test of the crystal-shape change.

Pyroelectric effect

The thermally activated structural variation in the polar molecules leads to a change in molecular dipole moment. Due to the uniaxial molecular packing along the crystallographic *c*-axis, the variation in the molecular polarization can transmit to the macroscopic polarization change of bulk single crystals. To investigate the change in the polarization of **1**, the pyroelectric measurement was performed using a Keithley 6517B electrometer equipped with a Quantum Design MPMS XL7 working as a temperature controller (Fig. S12 and S13†).

As shown in Fig. 5a and S13,† the pyroelectric current of compound **1** showed a non-zero value upon cooling and featured two sharp peaks in the vicinity of phase transition points along the polar axis of the single crystal. The continuous pyroelectric current above 130 K is ascribed to the gradual scissor-like motion of the coordination geometry that modifies the dipole moment of polar molecules. The calculated pyroelectric coefficients with values of *ca.* 1.5 nC K^{-1} cm^{-2} above 130 K and 23.7/35.8 nC K^{-1} cm^{-2} near the phase transition points are in the same order of magnitude as the well-known pyroelectric materials such as PVDF,[1,49] and some molecule-based crystal materials.[50] To obtain the change in polarization, the integration of the pyroelectric coefficient with respect to temperature was analysed. As shown in Fig. 5b, the polarization change (ΔP) gradually increased to 0.45 μC cm^{-2} upon further heating, with a two-step abrupt change found in the temperature range between 90 and 130 K. The polarization change of **1** is comparable to non-ferroelectric molecular compounds such as spin-crossover (SCO) molecular crystals ($[Fe(L)_2(ClO_4)_2]$ (L = propyl-2,6-di(1*H*-pyrazol-1-yl)isonicotinate), $\Delta P = 0.45$ μC cm^{-2}).[51]

To support the structural origin of the pyroelectric current, we investigated the variation in the molecular dipole moment corresponding to the scissor-like motion with density functional theory (DFT) calculations. The calculation results revealed that the dipole moments of part B in the disordered structure are 14.877 D (90 K) and 16.020 D (260 K) (Fig. 5c), and the dipole moments of part A are 16.454 D (90 K) and

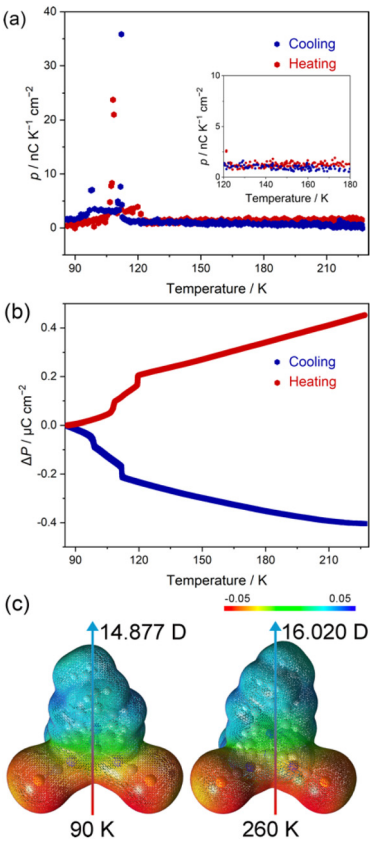

Fig. 5 Pyroelectric effect of compound **1**. (a) Pyroelectric coefficient (p). (b) Polarization change (ΔP). (c) Dipole moment of the structure of part B, in which the red area represents the negative charge and the blue area represents the positive charge.

16.989 D (260 K) (Fig. S14†). When the SOF of parts A and B was taken into account, a total polarization change of *ca.* 0.18 μC cm^{-2} can be obtained, suggesting that the constant pyroelectric coefficient is coupled with the gradual scissor-like motion of the complex. The calculated value is smaller than the experimental result, implying a substantial contribution of the secondary pyroelectric effect in the material.[1]

To further verify the influence of the scissor-like motion on the pyroelectric effect, two analogous compounds, namely, [Zn(4-isopropylpyridine)$_2$(NCS)$_2$] (**2**) and [Zn(4-*tert*-butylpyridine)$_2$(NCS)$_2$] (**3**) were investigated. These isostructural compounds crystallize in the polar *Fdd*2 space group, too (Table S2†). As shown in Fig. S15,† compounds **2** and **3** showed a slight structural change as the temperature changes. The crystallography *c*-axis expanded from 5.6808(5) Å (**2**) and 5.8157(2) Å (**3**) at 120 K to 5.8551(3) Å (**2**) and 5.9561(2) Å (**3**) at 340 K, indicating *ca.* 3.0% (**2**) and 2.4% (**3**) expansion along the *c*-axis, respectively. As a result, small thermal expansions with linear thermal expansion coefficients of 68 × 10^{-6} K^{-1} (**2**, Fig. S16†) and 82 × 10^{-6} K^{-1} (**3**, Fig. S17†) were detected along the polar axis, and no substantial pyroelectric current can be found in these compounds (Fig. S18†). These results further confirm that the giant anisotropic thermal expansion along with the macroscopic polarization change of compound **1** is associated with the scissor-like motion of the complex.

Conclusions

In summary, we demonstrated that a flexible Zn(II) single crystal shows giant anisotropic thermal expansion associated with a macroscopic polarization change. Detailed structural analyses disclosed that these unusual properties are associated with the scissor-like motion of the polar complex induced by a thermal dynamic state change of 4-ethylpyridine ligands. The molecular level structural changes are directly transmitted to the bulk materials due to the uniaxially aligned molecules in the polar crystal. Consequently, a remarkably large reversible shape change (*ca.* 10% along the long axis of the rod-like single crystal) associated with a pyroelectric current with a peak value of 35.8 nC K^{-1} cm^{-2} at the phase transition point was detected. The thermally driven obvious shape change and pyroelectric current in this non-ferroelectric molecular crystal suggest that **1** may find many applications in sensor elements.

Author contributions

Tao J. and Yao Z. S. proposed the strategy and supervised the experiments; Tang Z. and Yao Z. S. wrote the paper. Tang Z. performed the experiments, data preparation and analysis; Liu C. D. and Zhang Y. contributed to the pyroelectric measurement; Sun X. P. refined the structures; all authors contributed to the general discussion.

Conflicts of interest

There are no conflicts to declare.

Acknowledgements

This work was supported by the National Natural Science Foundation of China (22071009, 92061106, and 21971016) and Beijing Institute of Technology Research Fund Program for Young Scholars. The technical support from the staff at the Analysis & Testing Center, Beijing Institute of Technology is also appreciated.

Notes and references

1 M. E. Lines and A. M. Glass, *Principles and Applications of Ferroelectrics and Related Materials*, Oxford University Press, Oxford, 1977.
2 C. R. Bowen, J. Taylor, E. LeBoulbar, D. Zabek, A. Chauhan and R. Vaish, Pyroelectric materials and devices for energy harvesting applications, *Energy Environ. Sci.*, 2014, **7**, 3836–3856.

3 H. He, X. Lu, E. Hanc, C. Chen, H. Zhang and L. Lu, Advances in lead-free pyroelectric materials: a comprehensive review, *J. Mater. Chem. C*, 2020, **8**, 1494–1516.
4 K. W. Zhang, Y. B. Wang, Z. L. Wang and Y. Yang, Standard and figure-of-merit for quantifying the performance of pyroelectric nanogenerators, *Nano Energy*, 2019, **55**, 534–540.
5 D. Zhang, H. T. Wu, C. R. Bowen and Y. Yang, Recent Advances in Pyroelectric Materials and Applications, *Small*, 2021, **17**, 2103960.
6 A. Hossain and M. H. Rashid, Pyroelectric Detectors and their Applications, *IEEE Trans. Ind. Appl.*, 1991, **27**, 824–829.
7 X. Y. Li, S. G. Lu, X. Z. Chen, H. M. Gu, X. S. Qiana and Q. M. Zhang, Pyroelectric and electrocaloric materials, *J. Mater. Chem. C*, 2013, **1**, 23–37.
8 R. A. Kishore and S. Priya, A Review on Low-Grade Thermal Energy Harvesting: Materials, Methods and Devices, *Materials*, 2018, **11**, 1433.
9 P. Lheritier, A. Torelló, T. Usui, Y. Nouchokgwe, A. Aravindhan, J. N. Li, U. Prah, V. Kovacova, O. Bouton, S. Hirose and E. Defay, Large harvested energy with nonlinear pyroelectric modules, *Nature*, 2022, **609**, 718–721.
10 P. P. Shi, Y. Y. Tang, P. F. Li, W. Q. Liao, Z. X. Wang, Q. Ye and R. G. Xiong, Symmetry breaking in molecular ferroelectrics, *Chem. Soc. Rev.*, 2016, **45**, 3811–3827.
11 S. Horiuchi and Y. Tokura, Organic ferroelectrics, *Nat. Mater.*, 2008, **7**, 357–366.
12 J. Harada, Y. Kawamura, Y. Takahashi, Y. Uemura, T. Hasegawa, H. Taniguchi and K. Maruyama, Plastic/Ferroelectric Crystals with Easily Switchable Polarization: Low-Voltage Operation, Unprecedentedly High Pyroelectric Performance, and Large Piezoelectric Effect in Polycrystalline Forms, *J. Am. Chem. Soc.*, 2019, **141**, 9349–9357.
13 T. Hang, W. Zhang, H. Y. Ye and R. G. Xiong, Metal-organic complex ferroelectrics, *Chem. Soc. Rev.*, 2011, **40**, 3577–3598.
14 W. Zhang and R. G. Xiong, Ferroelectric Metal-Organic Frameworks, *Chem. Rev.*, 2012, **112**, 1163–1195.
15 A. S. Tayi, A. Kaeser, M. Matsumoto, T. Aida and S. I. Stupp, Supramolecular ferroelectrics, *Nat. Chem.*, 2015, **7**, 281–294.
16 A century of ferroelectricity, *Nat. Mater.*, 2020, **19**, 129.
17 J. F. Scott, Applications of Modern Ferroelectrics, *Science*, 2007, **315**, 954–959.
18 Z.-S. Yao, K. Yamamoto, H.-L. Cai, K. Takahashi and O. Sato, Above Room Temperature Organic Ferroelectrics: Diprotonated 1,4-Diazabicyclo[2.2.2]octane Shifts between Two 2-Chlorobenzoates, *J. Am. Chem. Soc.*, 2016, **138**, 12005–12008.
19 A. S. Tayi, A. K. Shveyd, A. C. H. Sue, J. M. Szarko, B. S. Rolczynski, D. Cao, T. J. Kennedy, A. A. Sarjeant, C. L. Stern, W. F. Paxton, W. Wu, S. K. Dey, A. C. Fahrenbach, J. R. Guest, H. Mohseni, L. X. Chen, K. L. Wang, J. F. Stoddart and S. I. Stupp, Room-temperature ferroelectricity in supramolecular networks of charge-transfer complexes, *Nature*, 2012, **488**, 485–489.
20 S. Horiuchi, K. Kobayashi, R. Kumai, N. Minami, F. Kagawa and Y. Tokura, Quantum ferroelectricity in charge-transfer complex crystals, *Nat. Commun.*, 2015, **6**, 7469.
21 N. Castagnetti, M. Masino, C. Rizzoli, A. Girlando and C. Rovira, Mixed stack charge transfer crystals: Crossing the neutral-ionic borderline by chemical substitution, *Phys. Rev. Mater.*, 2018, **2**, 024602.
22 K. Kobayashi, S. Horiuchi, R. Kumai, F. Kagawa, Y. Murakami and Y. Tokura, Electronic Ferroelectricity in a Molecular Crystal with Large Polarization Directing Antiparallel to Ionic Displacement, *Phys. Rev. Lett.*, 2012, **108**, 237601.
23 X. L. Wang, J. P. Xue, X. P. Sun, Y. X. Zhao, S. Q. Wu, Z. S. Yao and J. Tao, Giant Single-Crystal Shape Transformation with Wide Thermal Hysteresis Actuated by Synergistic Motions of Molecular Cations and Anions, *Chem. – Eur. J.*, 2020, **26**, 6778–6783.
24 Z.-S. Yao, M. Mito, T. Kamachi, Y. Shiota, K. Yoshizawa, N. Azuma, Y. Miyazaki, K. Takahashi, K. Zhang, T. Nakanishi, S. Kang, S. Kanegawa and O. Sato, Molecular motor-driven abrupt anisotropic shape change in a single crystal of a Ni complex, *Nat. Chem.*, 2014, **6**, 1079–1083.
25 N. C. Burtch, S. J. Baxter, J. Heinen, A. Bird, A. Schneemann, D. Dubbeldam and A. P. Wilkinson, Negative Thermal Expansion Design Strategies in a Diverse Series of Metal-Organic Frameworks, *Adv. Funct. Mater.*, 2019, **29**, 1904669.
26 Z. S. Yao, H. X. Guan, Y. Shiota, C. T. He, X. L. Wang, S. Q. Wu, X. Y. Zheng, S. Q. Su, K. Yoshizawa, X. Q. Kong, O. Sato and J. Tao, Giant anisotropic thermal expansion actuated by thermodynamically assisted reorientation of imidazoliums in a single crystal, *Nat. Commun.*, 2019, **10**, 4805.
27 S.-Q. Wu, M. Liu, K. Gao, S. Kanegawa, Y. Horie, G. Aoyama, H. Okajima, A. Sakamoto, M. L. Baker, M. S. Huzan, P. Bencok, T. Abe, Y. Shiota, K. Yoshizawa, W. Xu, H.-Z. Kou and O. Sato, Macroscopic Polarization Change via Electron Transfer in a Valence Tautomeric Cobalt Complex, *Nat. Commun.*, 2020, **11**, 1992.
28 S.-Q. Su, T. Kamachi, Z.-S. Yao, Y.-G. Huang, Y. Shiota, K. Yoshizawa, N. Azuma, Y. Miyazaki, M. Nakano, G. Maruta, S. Takeda, S. Kang, S. Kanegawa and O. Sato, Assembling an alkyl rotor to access abrupt and reversible crystalline deformation of a cobalt(II) complex, *Nat. Commun.*, 2015, **6**, 8810.
29 O. Sato, Dynamic molecular crystals with switchable physical properties, *Nat. Chem.*, 2016, **8**, 644–656.
30 Y. Li, B. Zhao, J.-P. Xue, J. Xie, Z.-S. Yao and J. Tao, Giant single-crystal-to-single-crystal transformations associated with chiral interconversion induced by elimination of chelating ligands, *Nat. Commun.*, 2021, **12**, 6908.
31 C. Wu, K.-G. Gao, Z.-S. Yao and J. Tao, A series of dynamic single crystals of $[M^{II}(en)_3]$ SO_4 (M = Ni, Mn, and Cd) shows tunable dielectric properties and anisotropic thermal expansion, *Dalton Trans.*, 2022, **51**, 6809–6816.

32 Z. Tang, X.-P. Sun, S.-D. Wang, X.-Y. Ji, Y. Li, Z.-S. Yao and J. Tao, Altering elastic-plastic mechanical response of a series of isostructural metal-organic complexes crystals, *Sci. China Chem.*, 2022, **65**, 710–718.
33 G. M. Sheldrick, Crystal structure refinement with SHELXL, *Acta Crystallogr., Sect. C: Struct. Chem.*, 2015, **C71**, 3–8.
34 O. V. Dolomanov, L. J. Bourhis, R. J. Gildea, J. A. Howard and H. Puschmann, OLEX2: a complete structure solution, refinement and analysis program, *J. Appl. Crystallogr.*, 2009, **42**, 339–341.
35 H. Chung, D. Dudenko, F. Zhang, G. D'avino, C. Ruzié, A. Richard, G. Schweicher, J. Cornil, D. Beljonne and Y. Geerts, Rotator side chains trigger cooperative transition for shape and function memory effect in organic semiconductors, *Nat. Commun.*, 2018, **9**, 278.
36 M. J. Cliffe and A. L. Goodwin, PASCal: a principal axis strain calculator for thermal expansion and compressibility determination, *J. Appl. Crystallogr.*, 2012, **45**, 1321–1329.
37 R. Guo, S. A. Markgraf, Y. Furukawa, M. Sato and A. S. Bhalla, Pyroelectric, dielectric, and piezoelectric properties of LiB_3O_5, *J. Appl. Phys.*, 1995, **78**, 7234–7239.
38 Y. Tang, L. Chen, X. Zhao, W. Jin and H. Luo, Anisotropic thermal expansion and phase transitions in $Pb(Mg_{1/3}Nb_{2/3})O_3$-0.3$PbTiO_3$ single crystals, *Phys. B*, 2006, **382**, 205–208.
39 J. D. Pang, C. P. Liu, Y. G. Huang, M. Y. Wu, F. L. Jiang, D. Q. Yuan, F. L. Hu, K. Z. Su, G. L. Liu and M. C. Hong, Visualizing the Dynamics of Temperature-and Solvent-Responsive Soft Crystals, *Angew. Chem., Int. Ed.*, 2016, **55**, 7478–7482.
40 Y.-G. Huang, Y. Shiota, M.-Y. Wu, S.-Q. Su, Z.-S. Yao, S. Kang, S. Kanegawa, G.-L. Li, S.-Q. Wu and T. Kamachi, Superior thermoelasticity and shape-memory nanopores in a porous supramolecular organic framework, *Nat. Commun.*, 2016, **7**, 11564.
41 D. Das, T. Jacobs and L. J. Barbour, Exceptionally large positive and negative anisotropic thermal expansion of an organic crystalline material, *Nat. Mater.*, 2010, **9**, 36–39.
42 T. Taniguchi, H. Sugiyama, H. Uekusa, M. Shiro, T. Asahi and H. Koshima, Walking and rolling of crystals induced thermally by phase transition, *Nat. Commun.*, 2018, **9**, 538.
43 Y. Duan, S. Semin, P. Tinnemans, H. Cuppen, J. Xu and T. Rasing, Robust thermoelastic microactuator based on an organic molecular crystal, *Nat. Commun.*, 2019, **10**, 4573.
44 E. Ahmed, D. P. Karothu, M. Warren and P. Naumov, Shape-memory effects in molecular crystals, *Nat. Commun.*, 2019, **10**, 3723.
45 D. P. Karothu, J. Weston, I. T. Desta and P. Naumov, Shape-memory and self-healing effects in mechanosalient molecular crystals, *J. Am. Chem. Soc.*, 2016, **138**, 13298–13306.
46 Y. G. Huang, Y. Shiota, S. Q. Su, S. Q. Wu, Z. S. Yao, G. L. Li, S. Kanegawa, S. Kang, T. Kamachi and K. Yoshizawa, Thermally Induced Intra-Carboxyl Proton Shuttle in a Molecular Rack-and-Pinion Cascade Achieving Macroscopic Crystal Deformation, *Angew. Chem., Int. Ed.*, 2016, **128**, 14848–14852.
47 C. Miller, D. Montgomery, M. Black and H. Schnetler, Thermal expansion as a precision actuator, *Proc. SPIE*, 2016, **9912**, 991269.
48 A. L. Goodwin, Organic Crystals Packing down, *Nat. Mater.*, 2010, **9**, 7–8.
49 R. W. Whatmore, Pyroelectric devices and materials, *Rep. Prog. Phys.*, 1986, **49**, 1335–1386.
50 P. Sadhukhan, S. Q. Wu, J. I. Long, T. Nakanishi, S. Kanegawa, K. G. Gao, K. Yamamoto, H. Okajima, A. Sakamoto, M. L. Baker, T. Kroll, D. Sokaras, A. Okazawa, N. Kojima, Y. Shiota, K. Yoshizawa and O. Sato, Manipulating electron redistribution to achieve electronic pyroelectricity in molecular FeCo crystals, *Nat. Commun.*, 2021, **12**, 4836.
51 S. Q. Su, S. Q. Wu, Y. B. Huang, W. H. Xu, K. G. Gao, A. Okazawa, H. Okajima, A. Sakamoto, S. Kanegawa and O. Sato, Photoinduced Persistent Polarization Change in a Spin Transition Crystal, *Angew. Chem., Int. Ed.*, 2022, **61**, e202208771.

